ADVANCED FUNCTIONAL MATERIALS
www.afm-journal.de

Hierarchical Graphene–Carbon Fiber Composite Paper as a Flexible Lateral Heat Spreader

Qing-Qiang Kong, Zhuo Liu, Jian-Guo Gao, Cheng-Meng Chen, Qiang Zhang, Guangmin Zhou, Ze-Chao Tao, Xing-Hua Zhang, Mao-Zhang Wang, Feng Li, and Rong Cai*

As a low dimensional crystal, graphene attracts great attention as heat dissipation material due to its unique thermal transfer property exceeding the limit of bulk graphite. In this contribution, flexible graphene–carbon fiber composite paper is fabricated by depositing graphene oxide into the carbon fiber precursor followed by carbonization. In this full-carbon architecture, scaffold of one-dimensional carbon fiber is employed as the structural component to reinforce the mechanical strength, while the hierarchically arranged two-dimensional graphene in the framework provides a convenient pathway for in-plane acoustic phonon transmission. The as-obtained hierarchical carbon/carbon composite paper possesses ultra-high in-plane thermal conductivity of 977 W m^{-1} K^{-1} and favorable tensile strength of 15.3 MPa. The combined mechanical and thermal performances make the material highly desirable as lateral heat spreader for next-generation commercial portable electronics.

1. Introduction

Efficient heat removal is a crucial issue for electronics and optoelectronics with increasing power densities based on recent progress on information, communication, and renewable energy technologies.[1,2] Thermal management, as highly required for next generation three-dimensional (3D) integration and ultra-fast high-power density transistors, is a decisive part for the performance and reliability of modern electronic, optoelectronic, photonic devices. As the heat dissipation ability of the basic device package is insufficient to control its temperature, advanced heat transfer materials, mainly including thermal interface materials (TIMs) and lateral heat spreaders, have become essential components for these systems.[3,4] Carbon allotropes and their derivatives occupy a unique place in terms of their unique ability to conduct heat.[4] For example, the thermal conductivity of one-dimensional (1D) carbon nanotubes (CNTs) is ~3000–3500 W m^{-1} K^{-1} at room temperature.[5,6] However, CNTs are not considered to be effective nano-fillers in terms of their high interfacial thermal resistance due to strong phonon scattering.[7–9] Alternatively, the room temperature thermal conductivity of two-dimensional (2D) graphene is estimated to be *ca.* 5300 W m^{-1} K^{-1}, far exceeding the bulk graphite limit of 2000 W m^{-1} K^{-1}.[3,10,11]

TIMs were used to fill the gaps to increase the thermal transfer efficiency between thermal transfer surfaces in microprocessors and heat sinks (high cross-plane thermal conductivity required). Attributing to the unique low-dimensional crystal structure, in recent years, graphene are intensively perused as novel carbon nano-fillers to enhance the thermal conductivities of polymeric composites as TIMs.[12–17] Though the addition of graphene sheets to different matrix materials brings the record-high enhancement of the effective thermal conductivity at the small filler loading fraction (<10 vol%), the ultimate property of graphene is still restricted in TIMs materials (1–10 W m^{-1} K^{-1}), which is attributed to the thermal boundary resistance at the graphene-matrix interface.[1]

Meanwhile, the lateral heat spreaders function by removing local hot spot *via* transferring heat along the basal plane of the paper (high in-plane conductivity preferred).[18] Nowadays, lateral heat spreaders are widely used in various commercial portable electronics such as smart phones, touch panels, and LED lamps with more condensedly packed integrated circuits.[19] The graphitized polymide paper and flexible graphite paper are typical commercial paper-like lateral heat spreaders. However, the heat transfer ability of flexible graphite paper (100–700 W m^{-1} K^{-1})[20] will not meet the heat removal requirement for next generation electronics. Though the thermal conductivity of

Q.-Q. Kong, Z. Liu, J.-G. Gao, Prof. C.-M. Chen, Dr. Z.-C. Tao, Dr. X.-H. Zhang, M.-Z. Wang, R. Cai
Key Laboratory of Carbon Materials
Institute of Coal Chemistry
Chinese Academy of Sciences
27 Taoyuan South Road, Taiyuan 030001, China
E-mail: ccm@sxicc.ac.cn
Prof. Q. Zhang
Beijing Key Laboratory of Green Chemical Reaction Engineering and Technology
Department of Chemical Engineering
Tsinghua University
Beijing 10084, China
G.-M. Zhou, Prof. F. Li
Shenyang National Laboratory for Materials Science
Institute of Metal Research
Chinese Academy of Sciences
Shenyang 100016, China

DOI: 10.1002/adfm.201304144

graphitized polyimide paper reaches around 1000 W m^{-1} K^{-1}, the cost is staying at a high level for indispensable graphitization over 3000 °C.[21] Therefore, a new low-cost lateral heat spreader with high thermal conductivity is always strongly considered. Fortunately, graphene based paper-like materials, with chemically derived graphene or functionalized graphene as the basic building blocks, have exhibited great potential as next generation lateral heat spreaders in recent reports.[22]

The graphene oxide papers assembled by solution based approaches showed good mechanical properties. However, the thermal and electronic conductivity are not satisfied due to the acoustic phonon scattering by interlayer interaction and the interruption of electron transfer by oxygen functionalities and lattice defects.[23] Though the conductive properties of the papers are restored by thermal annealing and/or chemical reduction, the mechanical performance of which drops simultaneously due to the random interlayer expansion during decomposition of functional sites.[24] The resulting material is very fragile and thus unfavorable for the further processing. Besides, the over compacted stacking of graphene in the film also increases the interlayer interference to the vibration induced phonon transfer, so as to restrain the performance of the resulting material. Therefore, how to combine ultrahigh thermal conductivity and extraordinary mechanical properties in a macroscopic graphene-based material is a great challenge.

In this contribution, a novel hierarchical graphene-carbon fiber (G-CF) composite paper was constructed for lateral heat transfer applications. The combination of 2D graphene and 1D CF, with two or more levels from the nanometer to the macroscopic scale, led to the formation of 3D hierarchical nanocomposites with unexpected performance.[25] Herein, the 1D CFs were selected as the scaffolds, not only to reinforce the mechanical stiffness and flexibility of the paper, but also to separate the graphene sheets from compactly re-stacking. Meanwhile, the individual graphene nanosheets, which were orderly interlinked in the 3D framework of CFs, provided a convenient pathway for in-plane heat transfer. The above carbon/carbon (C/C) composite paper exhibited ultrahigh thermal conductivities and mechanical properties and set new performance records.

2. Results and Discussion

As shown in **Figure 1**a, in a typical procedure, the polyacrylonitrile (PAN) derived CFs with an average length of 10 mm were homogeneously dispersed in aqueous solution with the assistance of polyacrylamide (PAM) as the dispersant and polyvinyl

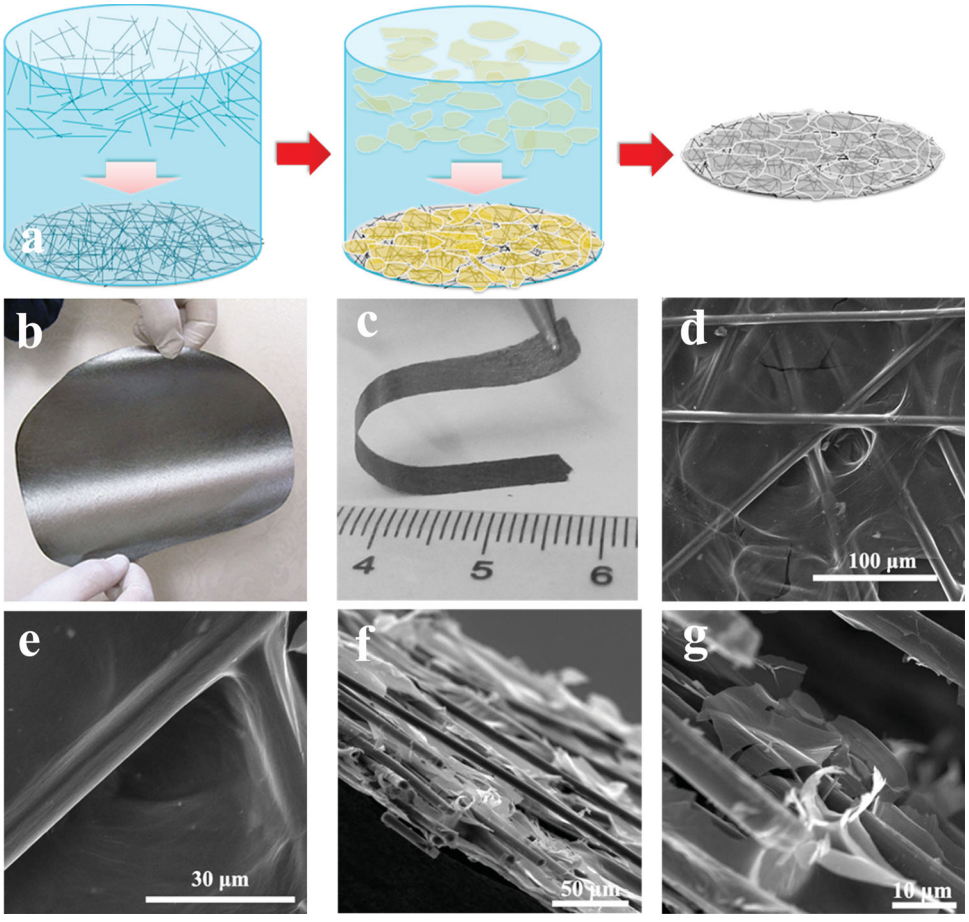

Figure 1. (a) Schematic diagram of the fabrication of GO-CF paper; (b,c) the digital image of G-CF paper; (d,e) SEM images (in plane); (f,g) SEM images (cross section).

alcohol (PVA) as the adhesive, respectively. Afterwards, the 3D porous CF scaffold was obtained by random deposition of the CFs on the porous metal plates through vacuum filtration. As the feedstock, graphene oxide (GO) was filled and deposited on the scaffold by a secondary micro-filtration of the GO hydrogel to form a GO-CF paper. Finally, the G-CF paper was available by hot press and subsequent thermal annealing at 1000 °C in Ar atmosphere. In the carbonization process, the GO was thermally reduced into graphene, while the PAM and PVA were simultaneously pyrolyzed. As shown in Figure 1b and c, the as-prepared G-CF paper with a diameter of 200 mm affords a typical metallic luster with superior toughness and flexibility.

The microstructure of the material was observed by scanning electron microscopy (SEM). The CF scaffold was homogeneously encapsulated by graphene nanosheets as a thin and uniform film on the surface (Figure 1d and e). Meanwhile, the cross-sectional images (Figure 1f and g) indicated that graphene nanosheets were sandwiched at the interlayer space of the frameworks with almost every CF was fully covered. With the assistance of vacuum induced directional flow of water, graphene nanosheets and CFs were stacked layer by layer to form an anisotropy concrete-like structure, in which CFs served as the reinforcing steel bar, while graphene sheets acted as the cement.

X-ray diffraction (XRD) was employed to investigate the structure evolution from GO-CF to G-CF. As shown in **Figure 2**a, there were three characteristic diffraction peaks in the patterns of GO-CF. The peak at 10.8 °C was attributed to GO while peaks at 20.0° and 22.3° were attributed to PVA, respectively.[26–28] After carbonization, the characteristic diffraction peaks of GO and PVA were disappeared which indicated well thermal reduction of GO and pyrolysis of PVA. Meanwhile, a new peak came out at 26.5°. The peak position was the same as that of reduced-graphene oxide (rGO). In contrast, the diffraction intensity was lower than that of rGO, which was ascribed to the spacer effect of CFs by preventing graphene sheets from over compacted stacking. The texture of the composite paper was further investigated by Raman spectroscopy (Figure 2b). It is noteworthy that the I_D/I_G ratio was increased from 0.95 of GO-CF to 1.16 of G-CF which was owing to the desorption of oxygen bonded saturated sp^3 carbons as CO_2 and CO. Various topological defects and vacancies were generated in the graphene lattice.[29] The thermal reduction of GO-CF was determined by Fourier transform infrared spectroscopy (FT-IR) spectra. As shown in Figure 2c, the peaks at 1080 (υ C-O), 1624 (δ C = C), 1730 (υ C = O), and 3411 cm^{-1} (υ O-H) were nearly disappeared and the G-CF sample behave somewhat infrared inert. Besides, the evolution of functionalities was further confirmed by elemental analysis (Table S1), as the C/O atomic ratio was increased from 2.33 of GO-CF to 50.50 of G-CF.

The thermochemistry of GO-CF composite paper, GO, CF, and PVA were further analyzed by thermogravimetric analysis in Ar atmosphere. As shown in Figure 2d, the mass loss of GO-CF was divided into four stages as follow: (I) from 30 to

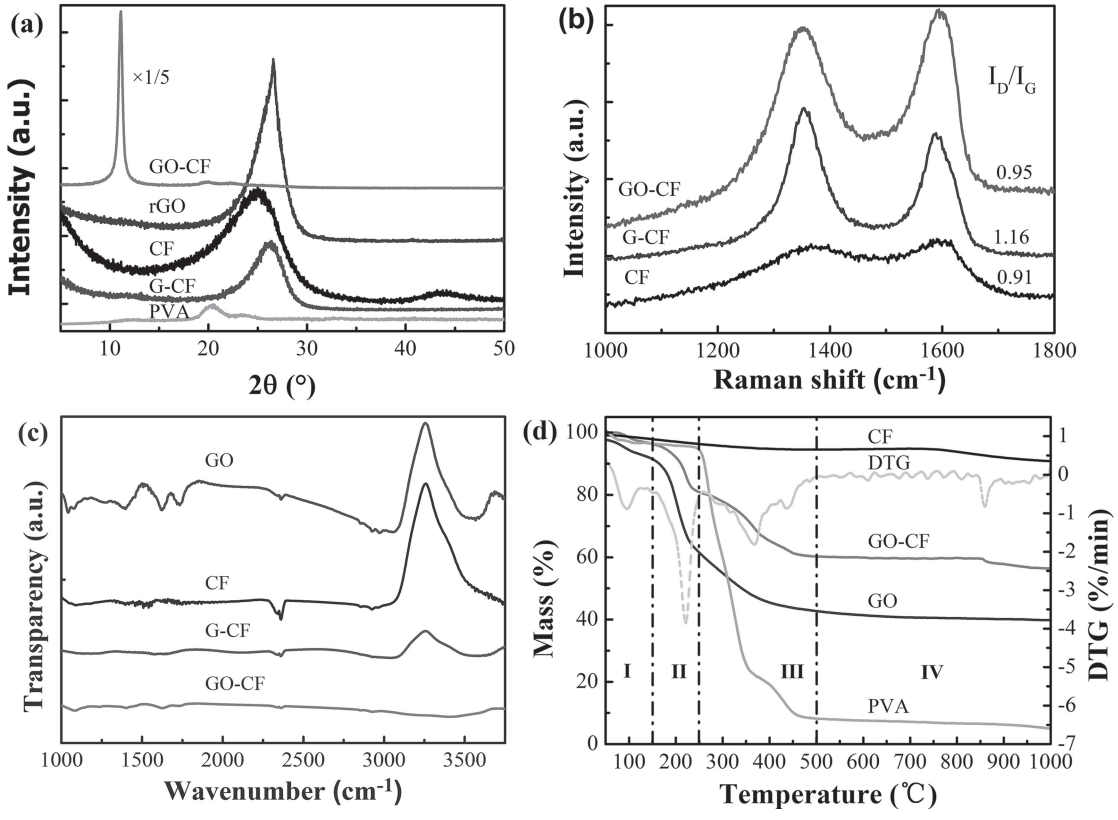

Figure 2. (a) XRD patterns of CF, rGO, PVA, GO-CF and G-CF paper; (b) Raman spectrum of CF, GO-CF and G-CF paper; (c) FT-IR spectrum of GO, CF, GO-CF and G-CF paper; (d) TG- analysis of GO-CF, GO, CF and PVA, and the DTG curves of GO-CF.

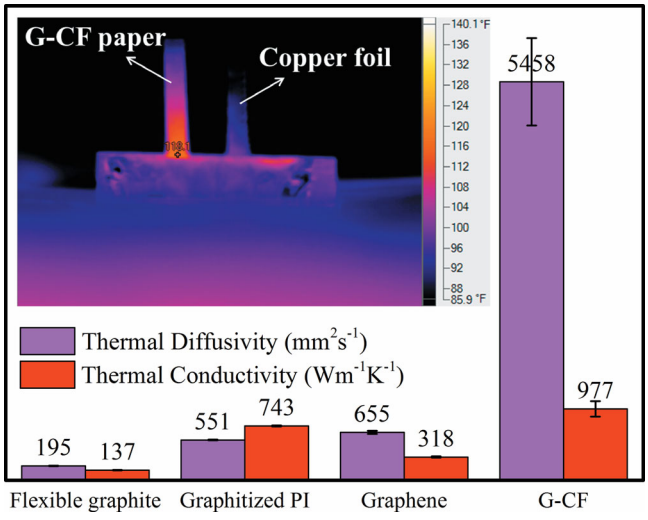

Figure 3. Thermal property of flexible graphite paper graphitized PI paper, graphene paper and G-CF paper. Inset shows the comparation of thermal conduction between G-CF paper and copper foil.

150 °C, the physically adsorbed water of GO was evaporated;[30] (II) from 150 to 250 °C, H_2O was generated from the intermolecular dehydration between neighboring carboxylic and/or hydroxyl groups of GO. Meanwhile, a fraction of CO and CO_2 were released from the decarboxylation reaction;[31] (III) from 250 to 500 °C, PVA was decomposed into abundant CO and CO_2. Besides, CO and CO_2 were released from the decomposion of anhydrides and phenols of GO;[32] (IV) from 500 to 1000 °C, residual oxygen- and nitrogen-containing functional groups in CF were removed steadily.[33] From the TG curve of CF, it can be seen that the mass loss of CF was slight from 30 to 1000 °C, and the major mass loss occured from 750 to 1000 °C was due to the remove of oxygen- and nitrogen-containing functional groups. A sharp mass loss of PVA occured at the stage of 250 to 500 °C, which was ascribed to the pyrolyzation process, and PVA was almost fully removed after carbonization at 1000 °C, so as to exclude its effect on the G-CF composite paper.

The thermal transport performances of G-CF paper and commercial copper foil were characterized by infrared thermal imaging spectrometer. As shown in the inset of **Figure 3**, after attached to the copper substrate for 1 minute, the temperature distribution on G-CF paper was significantly different from that of copper foil. G-CF paper transferred heat in higher efficiency to the surrounding environment compared to copper foil. Heat conduction in carbon materials is dominated by phonons, as the strong covalent sp^2 bonding and the small mass of carbon atoms resulting in efficient heat transfer by lattice vibrations.[4] While in the condition of metals, thermal conductivity mainly comes from the contribution of large concentrations of free electrons, leaving the contribution of phonons limited to 1–2% of the total. The higher thermal conductivity efficiency of G-CF, compared to copper fiol, was reflectied qualitively in the inset of Figure 3.

The in-plane thermal diffusivity of G-CF paper as well as flexible graphite paper, graphitized polymide (PI) paper[34] and graphene paper was further determined at room temperature using laser flash method. As shown in Figure 3, the in-plane thermal conductivity of G-CF paper is as high as 977 W m^{-1} K^{-1}, which is considerably larger than that of compactly stacked graphene paper (318 W m^{-1} K^{-1}) as well as commercial lateral heat spreader materials such as flexible graphite paper (137 W m^{-1} K^{-1}) and graphitized PI paper (743 W m^{-1} K^{-1}). Table S2 provides the detailed information about the thermal properties of every sample employed in this research.

We insist that the high thermal conductivity of G-CF paper attributes from the separated graphene sheets. On one hand, the thermal conductivity of PAN based carbon fibers selected in this contribution is as low as 10.5 W m^{-1} K^{-1} at room temperature. The overlap of chopped carbon fibers induces larger interfacial thermal resistance that further decreases the thermal conductivity of carbon fiber paper. Zamel et al.[35] measured the in-plane thermal conductivity of carbon fiber paper in the temperature of –20 to 120 °C. The thermal conductivity lied in the range of 11–26 W m^{-1} K^{-1}. On the other hand, previously studies[10,36] indicated that when graphene sheets were over compacted stacked into a paper, its thermal conductivity was greatly dropped by one order of magnitude due to the phonons leakage across the interface and the enhanced Umklapp scattering of out-of-plane acoustic (ZA) phonons. However, graphene sheets in G-CF paper are partly separated by CFs that effectively retards the stacking induced by the strong interlayer interactions. Thus phonons transfer thermal energy in strictly 2D channel with the interference from out-of-plane being eliminated. Consequently, the ultimate lateral heat transfer ability of graphene sheets in G-CF paper was expressed in a huge extent. Strong anisotropic thermal transfer performance was generated with significantly lower out-of-plane thermal conductivity of only 0.38 W m^{-1} K^{-1}, and this is in accordance with the highly orientation morphology under the directional filtration force, as shown in Figure 1f.

Further experiments showed that increased amounts of GO in the composite paper, with fixed mass of CF, resulted in decreased thermal conductivity (Table S3). This tendency also verified the importance of CF in separating over stacked graphene. Skeleton volume was maintained by fixed mass of CF. Certain part of graphene sheets were used to filling up the skeleton gap, while the rest part stacked over the surface of CF skeleton. The latter part accumulated layer-by-layer under vacuum filtration without separation of CF, and this layer was analogous to the pure graphene paper. So it is concluded that the introduction of CF gives full play to the excellent thermal properties of graphene. The mass ratio of CF to graphene is critical to obtain optimal thermal conductivity of G-CF paper: excess amount of graphene sheets lead to over stack, which enhances the phonon leakage and Umklapp scattering; inadequate amount of graphene cannot fulfill the skeleton gap of CF, and interlocking-tile structure cannot be formed to maintain the mechanical strength.

In order to evaluate the potential applications for G-CF paper, the mechanical properties of G-CF paper were investigated by bending and tensile test. In the case of bending test, the morphology and structure of G-CF remain unchanged after 6000 times of cycling. Meanwhile, the electric conductivity of G-CF paper was measured during the bending test. As shown in **Figure 4**a, the electric conductivity of G-CF has a positive correlation with the thermal conductivity fluctuates around 200 S cm^{-1}. According to Figure 4b, there is a linear relationship between tensile stress and strain at the first stage. The tensile strength

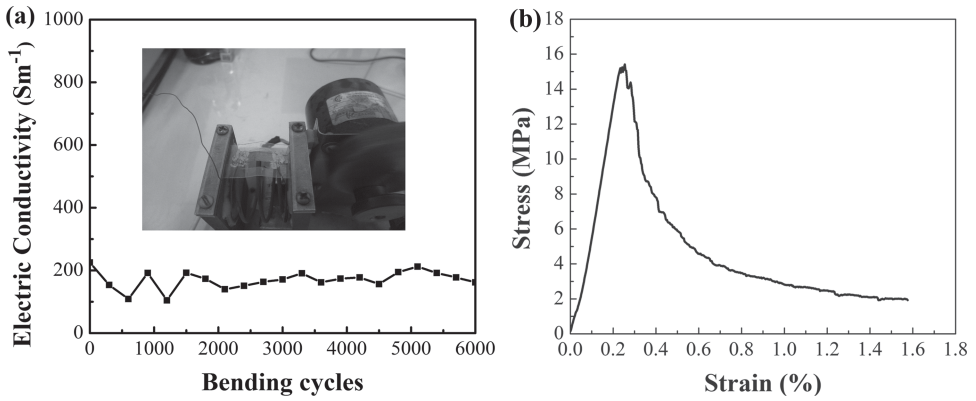

Figure 4. (a) Cycling performance of electric conductivity of the G-CF paper. Inset shows the laboratory apparatus for bending conductivity test; (b) Stress-strain plots of the G-CF paper.

and elastic modulus are evaluated to be ~15.2 MPa and ~6.5 GPa, respectively. The values are much larger than that of commercial flexible graphite paper (~10 MPa).[20] Moreover, it is noteworthy that the G-CF paper owns better flexibility than graphene paper, as shown in Figure 1b and c. The breakage of composite paper occurred in the bridged part of graphene nanosheets, which indicates that the stacking of graphene nanosheets is the origin of improved flexibility, and the framework of chopped CF contributes to the high tensile strength of the composite paper. The combination of stacking unit and framework was realized by vacuum filtration assembly. In Figure 1d and e, it can be seen that CF was tightly wrapped by flexible graphene sheets, forming a special interlocking-tile structure. The grapnene sheets, at the overlap joint, changed their lateral flatness to catch up with the bulging part of CF, while the rest part of graphene sheets remains stacked with each other. Increased interaction surface was yielded in G-CF composite compared with pure graphene paper, resulting in improved mechanical performance.

3. Conclusions

G-CF composite paper with ultrahigh thermal conductivity and excellent mechanical properties, can be produced through the combination of graphene and CFs. Graphene sheets serve as the functional part to provide high thermal conductivity while CFs function as the structural part to provide mechanical properties. Further investigation of the heat transfer mechanics in the nanostructured 3D architecture of graphene and CFs is necessary for designing advanced thermal transfer materials with much improved performance. Nevertheless, it is remarkable that the rising graphene and traditional CFs can be combined together with a relatively simple processing to obtain G-CF composite paper, which shows highly valuable in thermal management.

4. Experimental Section

4.1. Synthesis

GO: Graphite oxide was obtained by the method that has been reported in a previous publication.[37] The GO suspension in water (3.0 mg mL^{-1}) was treated in an ultrasonic cleaner (100 W) for 30 min, followed by centrifugation (5000 rpm, 10 min) to remove impurities.

CF Paper: Chopped CFs (length 10 mm, weight 200 mg), PAM (weight 100 mg), and PVA (weight 500 mg) were mixed in water with mild stirring for 30 min. Then the dispersion was filtered into a cake of 200 mm in diameter with the assistant of vacuum, followed by drying at 85 °C in vacuum for 3 min.

G-CF Composite Paper: The prepared GO suspension and CF paper was vacuum-filtrated with a vacuum system equipped with a nylon-6 filtration paper (40 μm pore size). The obtained filtration cake is carefully dried and hot pressed at 105 °C for 5 h, followed by thermal treatment at 1000 °C in Ar atmosphere for 1 h.

Flexible Graphite Paper: Flexible graphite paper was obtained by the method in the previous literature.[20,38] Natural flake graphite was intercalated with a mixture of perchloric acid and nitric acid. Then, it was exfoliated at 900 °C for 30 s. Subsequently, the exfoliated graphite was compressed in a steel mould and rolled to form flexible graphite paper with a thickness of 0.15–2.0 mm.

Graphitized PI Paper: Graphitized PI paper was obtained from polyimide films (Kapton, bought from DuPont Company) via graphitization at 3000 °C for 1 h. The details of the preparation were described in a previous publication.[39,40]

Copper Foil: Copper foil, with a thickness of 40 μm, was bought from Guangdong Meiyan electrolysis copper foil Ltd.

4.2. Characterization

The morphologies of G-CF were characterized by a JEOL JSM 7401F SEM operated at 3.0 kV. XRD (X-ray powder diffraction, $\lambda = 0.15406$ nm, Xpert PRO, PHYILIPS) with Cu K_α radiation was performed in the range of 5–50°. Laser Raman spectroscopy was performed by using Horiba Jobin Yvon LabRAM HR800 Raman spectrometer with He-Ne laser excitated at 633 nm. FT-IR was obtained on a Bruker Tensor 27 and the sample was pre-pressed with KBr into pellets before test. The elemental analysis was conducted by Vario EL CUBE elemental analyzer. The TG analysis was carried out on a NETZSCH5 thermal gravimetric analysis (TGA) system in Ar atmosphere.

The heat transport property of Copper foil and G-CF paper were characterized by infrared thermal imaging spectrometer. The thermal diffusivity of all samples were further determined using Laser Flash Apparatus (NETZSCH LFA 447 *NanoFlash*) operated at room temperature in a vacuum of 0.01 Pa. In this method, the test sample was cut into round shape with diameter of 25.4 mm, as the sample carrier is standard with fixed size. First, the sample was heated by light pulse, and then the resulting temperature rise at four different positions is measured using infrared detector. The thermal diffusivity is determined by analyzing the temperature-versus-time curve based on the following equation:

$$D = 0.1388 \cdot d^2 \cdot t_{1/2}^{-1} \quad (1)$$

In Equation (1), D is the thermal diffusivity, d is the thickness of the tested sample and t is the diffusion time. Finally, the thermal conductivity (λ) was calculated using the Equation (2).

$$\lambda = \rho \cdot C_P \cdot D \quad (2)$$

Herein, ρ (2.295×10^{-4} g mm^{-3}) is the density of the composite paper, and C_P (0.780 J g^{-1} K^{-1}) is the specific heat capacity obtained by differential scanning calorimetry (DSC, NETZSCH DSC 200 F3 Maia). The density (ρ) in Equation (2) is obtained according to $\rho = m V^{-1}$, among which, m and V are the mass and volume of the sample, respectively. The mass was available by weighing the round sample with a diameter of 25.4 mm using electronic precision balance. The volume was determined by the products of flake area and thickness of the sample. The thickness was measured by ZH-4 paper and cardboard thickness detector working at specific contact area and pressure. The total thickness of ten pieces of composite paper was measured while the used thickness was received by dividing the total thickness with ten.

The specific heat capacity (C_P) was measured by DSC. The measurement was conducted using sapphire method according to Equation (3). Three tests including blank test, sapphire test, and sample test were carried out in turn. Firstly, the base curve of DSC was achieved by the blank test. The sapphire was selected as reference sample with known C_P. Then the DSC curves, heat enthalpy change rate dH/dt as a function of time t, of the sample and sapphire were calibrated with the base curve. Comparing the DSC signal of sample with that of sapphire, C_P of the being tested sample can be calculated based on the following equation:

$$\frac{DSC_{sample} - DSC_{bas}}{DSC_{standard} - DSC_{bas}} = \frac{Cp_{sample} \cdot m_{sample}}{Cp_{standard} \cdot m_{standard}} \quad (3)$$

DSC_{sample}, DSC_{bas}, $DSC_{standard}$ are the ordinate of the DSC curves corresponding to the sample, blank specimen, and standard specimen, respectively. $C_{Psample}$ and $C_{Pstandard}$ are the specific heat of the sample and standard specimen, respectively. m_{sample} and $m_{standard}$ are the mass of the sample and sapphire, respectively.

The stress-strain test was performed on a Hounsfield (HS5N) tensile tester with a strain rate of 0.1 mm min^{-1}. To examine the flexibility and durability of G-CF composite paper, a cyclic bend test was performed. The size of the G-CF paper used was 12.0 mm × 5.0 mm. During the bending test, the minimum radius of curvature was ~1.5 mm. The electrical conductivity of the G-CF paper during the bend test was measured synchronously.

Supporting Information

Supporting Information is available from the Wiley Online Library or from the author.

Acknowledgements

We acknowledge the financial support from the Innovative Research Fund of ICC-CAS (2012SCXQT03), Natural Science Foundation of China (51302281), Natural Science Foundation of Shanxi Province (2013011012–7), Innovative Research Fund of Taiyuan Science and Technology Bureau (2012CXJD0510), Shanxi Coal Transportation and Sales Group Co. Ltd (2013WT103).

Received: December 12, 2013
Revised: January 17, 2014
Published online: March 20, 2014

[1] K. M. F. Shahil, A. A. Balandin, *Solid State Commun.* **2012**, *152*, 1331.
[2] R. Goli, S. Legedza, A. Dhar, R. Salgado, J. Renteria, A. A. Balandin, *J. Power Sources* **2014**, *248*, 37.
[3] M. M. Sadeghi, M. T. Pettes, L. Shi, *Solid State Commun.* **2012**, *152*, 1321.
[4] A. A. Balandin, *Nat. Mater.* **2011**, *10*, 569.
[5] P. Kim, L. Shi, A. Majumdar, P. L. McEuen, *Phys. Rev. Lett.* **2001**, *87*, 215502.
[6] E. Pop, D. Mann, Q. Wang, K. Goodson, H. J. Dai, *Nano Lett.* **2006**, *6*, 96.
[7] L. M. Veca, M. J. Meziani, W. Wang, X. Wang, F. S. Lu, P. Y. Zhang, Y. Lin, R. Fee, J. W. Connell, Y. P. Sun, *Adv. Mater.* **2009**, *21*, 2088.
[8] S. Ghosh, I. Calizo, D. Teweldebrhan, E. P. Pokatilov, D. L. Nika, A. A. Balandin, W. Bao, F. Miao, C. N. Lau, *Appl. Phys. Lett.* **2008**, *92*, 151911.
[9] J. L. Xiang, L. T. Drzal, *Carbon* **2011**, *49*, 773.
[10] J. H. Seol, I. Jo, A. L. Moore, L. Lindsay, Z. H. Aitken, M. T. Pettes, X. S. Li, Z. Yao, R. Huang, D. Broido, N. Mingo, R. S. Ruoff, L. Shi, *Science* **2010**, *328*, 213.
[11] A. K. Geim, *Science* **2009**, *324*, 1530.
[12] W. L. Song, L. M. Veca, C. Y. Kong, S. Ghose, J. W. Connell, P. Wang, L. Cao, Y. Lin, M. J. Meziani, H. J. Qian, G. E. LeCroy, Y. P. Sun, *Polymer* **2012**, *53*, 3910.
[13] K. M. F. Shahil, A. A. Balandin, *Nano Lett.* **2012**, *12*, 861.
[14] T. F. Luo, J. R. Lloyd, *Adv. Funct. Mater.* **2012**, *22*, 2495.
[15] M. Terrones, O. Martín, M. González, J. Pozuelo, B. Serrano, J. C. Cabanelas, S. M. Vega-Díaz, J. Baselga, *Adv. Mater.* **2011**, *23*, 5302.
[16] H. Fukushima, L. T. Drzal, B. P. Rook, M. J. Rich, *J. Therm. Anal. Calorim.* **2006**, *85*, 235.
[17] K. Kalaitzidou, H. Fukushima, L. T. Drzal, *Carbon* **2007**, *45*, 1446.
[18] S. Subrina, *IEEE T. Nanotechnol.* **2012**, *11*, 777.
[19] Z. Yan, G. X. Liu, J. M. Khan, A. A. Balandin, *Nat. Commun.* **2012**, *3*, 827.
[20] X. H. Wei, L. Liu, J. X. Zhang, J. L. Shi, Q. G. Guo, *J. Mater. Sci.* **2010**, *45*, 2449.
[21] Y. Kaburagi, T. Kimuraa, A. Yoshidab, Y. Hishiyama, *Carbon* **2012**, *50*, 4984.
[22] S. Subrina, D. Kotchetkov, A. A. Balandin, *IEEE Electron Device Lett.* **2009**, *30*, 1281.
[23] J. Y. Kim, J. H. Lee, J. C. Grossman, *ACS Nano* **2012**, *6*, 9050.
[24] D. W. Wang, G. Zhou, F. Li, K. H. Wu, G. Q. Lu, H. M. Cheng, I. R. Gentle, *Phys. Chem. Chem. Phys.* **2012**, *14*, 8703.
[25] M. Q. Zhao, Q. Zhang, J. Q. Huang, F. Wei, *Adv. Funct. Mater.* **2012**, *22*, 675.
[26] X. B. Fan, W. C. Peng, Y. Li, X. Y. Li, S. L. Wang, G. L. Zhang, F. B. Zhang, *Adv. Mater.* **2008**, *20*, 4490.
[27] H. E. Assender, A. H. Windle, *Polymer* **1998**, *39*, 4295.
[28] A. J. Rodriguez, M. E. Guzman, C. S. Lim, B. Minaie, *Carbon* **2010**, *48*, 3256.
[29] C. M. Chen, Q. Zhang, M. G. Yang, C. H. Huang, Y. G. Yang, M. Z. Wang, *Carbon* **2012**, *50*, 3572.
[30] C. M. Chen, J. Q. Huang, Q. Zhang, W. Z. Gong, Q. H. Yang, M. Z. Wang, Y. G. Yang, *Carbon* **2012**, *50*, 659.
[31] W. Lv, D. M. Tang, Y. B. He, C. H. You, Z. Q. Shi, X. C. Chen, C. M. Chen, P. X. Hou, C. Liu, Q. H. Yang, *ACS Nano* **2009**, *3*, 3730.
[32] J. A. Menéndez, J. Phillips, B. Xia, L. R. Radovic, *Langmuir* **1996**, *12*, 4404.
[33] K. P. Loh, Q. L. Bao, P. K. Ang, J. X. Yang, *J. Mater. Chem.* **2010**, *20*, 2277.
[34] M. Inagaki, N. Ohta, Y. Hishiyama, *Carbon* **2013**, *61*, 1.
[35] N. Zamel, E. Litovsky, S. Shakhshir, X. G. Li, J. Kleiman, *Appl. Energ.* **2011**, *88*, 3042.
[36] D. Singh, J. Y. Murthy, T. S. Fisher, *J. Appl. Phys.* **2011**, *110*, 044317.

[37] C. M. Chen, Q. H. Yang, Y. G. Yang, W. Lv, Y. F. Wen, P. X. Hou, M. Z. Wang, H. M. Cheng, *Adv. Mater.* **2009**, *21*, 3007.
[38] X. H. Wei, L. Liu, J. X. Zhang, J. L. Shi, Q. G. Guo, *Mater. Lett.* **2009**, *63*, 1618.
[39] Y. Hishiyama, M. Nakamura, Y. Nagata, M. Inagaki, *Carbon* **1994**, *32*, 645.
[40] Y. Hishiyama, A. Yoshida, M. Inagaki, *Carbon* **1998**, *36*, 1113.